Prostate Spectroscopy at 3 Tesla Using Two-Dimensional S-PRESS

Thomas Lange, Andreas H. Trabesinger, Rolf F. Schulte, Ulrike Dydak, and Peter Boesiger*

Two-dimensional (2D) strong-coupling point-resolved spectroscopy (S-PRESS) is introduced as a novel approach to ^{1}H MR spectroscopy (MRS) in the prostate. The technique provides full spectral information and allows for an accurate characterization of the citrate (Cit) signal. The method is based on acquiring a series of PRESS spectra with constant total echo time (TE). The indirect dimension is encoded by varying the relative lengths of the first and second TEs ($TE_1 + TE_2 = TE$). In the resulting 2D spectra, only the signal of strongly coupled spin systems is spread into the second dimension, which leads to more clearly arranged spectra. Furthermore, the spectral parameters of Cit (coupling constant J and chemical shift difference δ of the AB spin system) can be determined with high accuracy in vivo. The sequence is analytically optimized for maximal "strong coupling peaks" of Cit at 3T. 2D S-PRESS spectra are compared with JPRESS spectra in vitro as well as in vivo.   Magn Reson Med 56:1220–1228, 2006. © 2006 Wiley-Liss, Inc.

Key words: S-PRESS; strong coupling; citrate; prostate; MRS

Because of its noninvasive nature, magnetic resonance imaging (MRI) has proven to be an indispensable method for diagnosing many pathologies, especially tumors. However, the morphological and relaxometric information provided by MRI is not sufficient for unequivocally diagnosing certain tumor types. In such cases MR spectroscopy (MRS) can provide valuable complementary metabolic information (1). For the diagnosis of prostate cancer, the metabolites choline (Cho) and citrate (Cit) are of particular interest (1,2). Cit is secreted in relatively large amounts by the epithelial cells of the prostate. High levels of zinc inhibit the oxidation of Cit in the Krebs cycle (3). However, in cancerous epithelial tissue the zinc concentration is considerably reduced, resulting in lower net Cit levels. On the other hand, the Cho concentration is increased due to the rapid cell turnover in tumorous tissue. Therefore, the Cho-to-Cit concentration ratio can help to discriminate between malignant adenocarcinoma and benign hyperplasia (2,4,5).

The preferred method for localized prostate ^{1}H MRS is the double spin-echo sequence called point-resolved spectroscopy (PRESS) (6). Because of its high signal yield (e.g., compared to stimulated-echo acquisition mode (STEAM) (7)), it is the method of choice, especially when surface coils are used for signal reception.

While the detection and quantification of the uncoupled Cho resonance is straightforward, Cit represents a strongly coupled AB spin system at typical field strengths available for in vivo MRS ($B_0 \leq 7$ T) and is therefore a challenge for spectroscopists. The strong coupling gives rise to a complicated J-modulation of the Cit resonance that critically depends on the sequence timing. Several groups have investigated the signal behavior of Cit and optimized the PRESS sequence to yield maximum signal intensity and a line-shape appropriate for Cit quantification (8–14).

Expanding PRESS to a second dimension has been shown to be useful for disentangling overcrowded spectra. A powerful method that enables the separation of chemical shift and coupling information for J-coupled metabolites is 2D J-resolved PRESS (JPRESS) (15). PRESS spectra are acquired with varying TEs, which encode the indirect t_1 dimension. The application of JPRESS in prostate examinations enables the spectral separation of creatine (Cr) and Cho from spermine (Spm), which has a similar resonance frequency (16,17). Kim et al. (18) combined JPRESS with spectroscopic imaging (SI) to identify the region of abnormal metabolism due to prostate cancer more accurately. The line-widths in the indirect dimension of JPRESS spectra are governed only by the T_2 decay—not by field inhomogeneities as in 1D spectra, where T_2^* determines the line-widths. Thus a better spectral resolution of coupled resonances is achieved. The possibility of determining T_2 values from 2D J-resolved spectra is an additional benefit.

However, strong scalar coupling leads to additional peaks in 2D spectra, which can complicate peak assignment and quantification (19). While weakly coupled two-spin systems give rise to four peaks in a JPRESS experiment, the Cit molecule shows a spectral pattern with eight peaks. The additional peaks stem from the coherence transfer between the coupled spins. Thrippleton et al. (19) suggested several methods for suppressing these strong coupling peaks in JPRESS experiments. One approach is a multiscan technique that employs an incremental simultaneous displacement of the two refocusing pulses within the sequence, leaving the total TE unchanged. Gambarota et al. (20) proposed a difference editing method based on the S-PRESS sequence. It uses PRESS localization ($90°_x$ - [$TE_1/2$] - $180°_y$ - [$TE_1/2 + TE_2/2$] - $180°_y$ - [$TE_2/2$] - Acq) and consists of two measurements with the same overall TE ($TE = TE_1 + TE_2$ = const), but with different TE_1 and TE_2. When the two resulting spectra are subtracted from each other, uncoupled and weakly coupled resonances are

suppressed, while the strong coupling peaks remain. At a field strength of 3T, density matrix simulations predicted a maximum *J*-modulation of Cit for a TE of 280 ms and helped to determine the optimal TE_1 values for difference editing.

In this work we combine the strengths of 2D spin-echo spectroscopy and the S-PRESS approach by implementing S-PRESS as a 2D technique. The method was analytically optimized for prostate MRS and validated in vitro as well as in vivo. 2D S-PRESS was used to determine the spectral parameters of Cit (*J* and δ) in vivo with relatively high precision.

THEORY

The ^{1}H MR signal of Cit arises from two magnetically equivalent methylene groups (CH_2) that constitute strongly coupled AB spin systems at currently available field strengths for in vivo MRS ($B_0 \leq 7$ T). In 1D PRESS the Cit resonance consists of four lines (Fig. 1) centered around 2.6 ppm. While the separation between the two leftmost and the two rightmost lines equals the field-independent coupling constant (*J* = 16.1 Hz), the distance between the two inner lines depends on the magnetic field strength, due to the linear field dependence of the chemical shift difference between the A and B spins (δ = 0.149 ppm) (21). As a characteristic feature of strongly coupled spin systems, the two inner lines show higher signal intensity than the two outer lines. Furthermore, the strong coupling causes a complicated amplitude and phase modulation of the Cit resonance as a function of TE. This behavior cannot be easily understood in the classic sense, and requires a quantum mechanical description. The Hamiltonian for an AB spin system can be written as

$$H = (\omega_A A_z + \omega_B B_z) + 2\pi J(A_x B_x + A_y B_y + A_z B_z), \quad [1]$$

where $A_{x,y,z}$ and $B_{x,y,z}$ are the angular momentum operators in Cartesian coordinates, ω_A and ω_B are the chemical shifts, and *J* is the coupling constant of the two coupled spins A and B. The nonsecular contribution $A_x B_x + A_y B_y$ is characteristic of strongly coupled spin systems and is usually neglected in the limit of weak scalar coupling. Writing this expression in terms of raising and lowering

operators yields $\frac{1}{2} \cdot (A_+ B_- + A_- B_+)$, indicating that there is a coherence transfer between spins A and B due to strong coupling. By analytically calculating the density matrix evolution with this Hamiltonian or applying the Kay-McClung formalism (22), the signal resulting from a PRESS sequence can be expressed in terms of four groups of Cartesian single-quantum coherence product operators $\{(A_y + B_y), (2A_x B_z + 2A_z B_x), (A_x - B_x), (2A_y B_z - 2A_z B_y)\}$ (12). The amplitudes of the detectable in-phase components $M_y = (A_y + B_y)/2$ and $M_x = (A_x - B_x)/2$ are listed in Table 1. Most amplitude terms only show a dependence on the total TE, but are independent of the particular choice of TE_1 and TE_2. However, the amplitude expressions also contain summands depending on the difference $TE_1 - TE_2$. These terms are characteristic for strongly coupled spin systems and vanish in the weak-coupling limit.

A 2D S-PRESS experiment consists of multiple PRESS measurements with a constant TE but a simultaneous incremental variation of TE_1 and TE_2. When TE_1 is encoded in the indirect dimension (t_1) and a 2D Fourier transformation is applied to the data, the resulting 2D spectrum displays the strong coupling information resolved in the indirect spectral dimension (f_1). Strongly coupled spin systems reveal a line-splitting in f_1, whereas uncoupled and weakly coupled metabolites resonate only at $f_1 = 0$ Hz. For AB spin systems, these strong coupling peaks arise from the terms depending on $TE_1 - TE_2$ in Table 1 and appear at frequencies $f_1 = \pm \Lambda/2$ Hz, where $\Lambda = \sqrt{\delta^2 + J^2}$. Since all acquired echo signals have undergone the same T_2 decay and are aligned along their echo tops in t_1, the spectral resolution in the indirect dimension of a 2D S-PRESS spectrum is limited only by the TE_1 encoding range, and not by field inhomogeneities or T_2 relaxation.

The signal intensity of the strong coupling S-PRESS peaks at $f_1 = \pm \Lambda/2$ shows a modulation with TE. It can be calculated as a function of TE from the amplitude terms given in Table 1, as shown in the Appendix. The strong coupling peaks even vanish for certain TEs (TE = {n · 2/Λ, n ϵ N}). This has to be taken into account when setting up a 2D S-PRESS experiment.

While the trigonometric factors in the amplitude terms (Table 1) can be adjusted and optimized via the TE, the polynomial factors depend only on the coupling strength $\kappa = J/\delta$ of the AB spin system, which can be shown with basic substitutions:
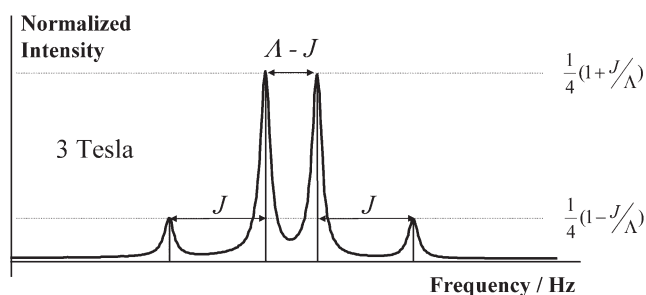

Normalized Intensity

3 Tesla

$\Lambda - J$

$\frac{1}{4}(1 + J/\Lambda)$

J   *J*

$\frac{1}{4}(1 - J/\Lambda)$

Frequency / Hz

FIG. 1. Plot of the Cit signal as obtained in a pulse-acquire experiment at 3T. *J* denotes the strength of the scalar coupling in Hz, and $\Lambda = \sqrt{\delta^2 + J^2}$ is the strong coupling frequency, where δ is the difference in Larmor frequencies between the two coupled protons. The total intensity is normalized to one.

$$P_{1,x} = 2J^2\delta/\Lambda^3 = \frac{2 \cdot \kappa^2}{(1 + \kappa^2)^{1.5}} \quad [2a]$$

$$P_{2,x} = 2J\delta/\Lambda^2 = \frac{2 \cdot \kappa}{1 + \kappa^2} \quad [2b]$$

$$P_{1,y} = 2J\delta^2/\Lambda^3 = \frac{2 \cdot \kappa}{(1 + \kappa^2)^{1.5}} \quad [2c]$$

Plotting these polynomial factors (Fig. 2) shows that they reach maxima for $\kappa_{max} = \sqrt{2}$, $\kappa_{max} = 1$ and $\kappa_{max} = 1/\sqrt{2}$, respectively. This means that the highest signal yield for S-PRESS experiments is achieved for spin systems with

Table 1
Analytical Calculation of Echo Signal in Response to the PRESS Sequence ($90°_x-[TE_1/2]-180°_y-[TE_1/2-TE_2/2]$ $-180°_y-[TE_2/2]-Acq$) (12)*

Operator	Amplitude
$M_y = (A_y + B_y)/2$	$-\cos(\pi J \cdot TE) \cdot [(\delta/\Lambda)^2 + (J/\Lambda)^2 \cos(\pi \cdot \Lambda \cdot TE)]$
$(B_y = A_y)$	$-\sin(\pi J \cdot TE) \cdot \left[(J/\Lambda)^3 \sin(\pi \cdot \Lambda \cdot TE) + (2J\delta^2/\Lambda^3)\sin\left(\frac{\pi}{2}\Lambda \cdot TE\right)\cos\left(\frac{\pi}{2}\Lambda \cdot (TE_1 - TE_2)\right) \right]$
$M_x = (A_x - B_x)/2$	$-\cos(\pi J \cdot TE) \cdot \left[(J^2\delta/\Lambda^3)\left(2\sin\left(\frac{\pi}{2}\Lambda \cdot TE\right)\cos\left(\frac{\pi}{2}\Lambda \cdot (TE_1 - TE_2)\right) - \sin(\pi \cdot \Lambda \cdot TE)\right) \right]$
$(B_x = -A_x)$	$-\sin(\pi J \cdot TE) \cdot \left[(2J\delta/\Lambda^2)\sin\left(\frac{\pi}{2}\Lambda \cdot TE\right)\sin\left(\frac{\pi}{2}\Lambda \cdot (TE_1 - TE_2)\right) \right]$

*Due to symmetry considerations the signal contributions can be subdivided into four groups of single-quantum coherence product operators {$(A_y + B_y)$, $(2A_xB_z + 2A_zB_x)$, $(A_x - B_x)$, $(2A_yB_z - 2A_zB_y)$}. Only the in-phase components are listed. J = strength of the scalar coupling, δ = difference in Larmor frequencies, $\Lambda = \sqrt{\delta^2 + J^2}$; $TE = TE_1 + TE_2$.

$\kappa = J/\delta \approx 1$, which is the case for Cit at a field strength of 3T.

The spectral parameters of Cit (J and δ) sensitively depend on the chemical environment. van der Graaf et al. (21) showed in phantom experiments that J and δ increase with the concentration of divalent cations, such as Mg^{2+}, Ca^{2+}, and Zn^{2+}. They also reported a strong dependence on the pH value. This raises the question as to whether there is a detectable difference in J and δ between cancerous and healthy tissues. The Zn^{2+} concentration plays a particularly important role in the pathophysiology of adenocarcinoma. It is largely reduced in cancerous tissue and may therefore be useful as a marker for prostate cancer. Prostate spectroscopy usually exploits the fact that zinc ions prevent Cit from being oxidized. A reduced Zn^{2+} concentration is accompanied by a diminished Cit level, which is detected in MRS experiments. Therefore, we carried out a phantom experiment to investigate whether this zinc decrease could be detected on the basis of changes in J and δ.

MATERIALS AND METHODS

All experiments were performed on a Philips Achieva 3T system (Philips Medical Systems, Best, The Netherlands). Phantom experiments were carried out with a transmit/receive head coil. All in vivo spectra were acquired with a two-element ellipsoidal surface coil (semi-major axis = 17 cm, semi-minor axis = 14 cm), and the body coil was used for transmission.

Both 2D S-PRESS and JPRESS measurements are based on the PRESS sequence:

$$90°_x - [TE_1/2] - 180°_y - [TE_1/2 + TE_2/2]$$
$$- 180°_y - [TE_2/2] - Acq. \quad [3]$$

The acquisition employed a maximum-echo sampling scheme (23,24) with 1024 sampling points covering a bandwidth of 2000 Hz. For both 2D S-PRESS and JPRESS experiments the measurement started with the manufacturer's default PRESS implementation, in which TE_1 is as short as possible. In the 2D S-PRESS experiments TE_1 and TE_2 were varied simultaneously to keep the total TE constant. TE_1 was encoded in the indirect t_1 dimension. For the JPRESS experiments, starting from the shortest possible TE, only TE_2 and hence the total TE were varied and encoded in the indirect t_1 dimension.

The water signal was suppressed with selective excitation in conjunction with gradient spoiling prior to the PRESS sequence. Band-selective inversion with gradient dephasing (BASING) further improved the water suppression for the 2D S-PRESS measurements (25,26). The combination of these two techniques suppressed the water resonance almost completely, and thus prevented folding artifacts from large water peak tails. Fat suppression was omitted because careful voxel selection ensured that no periprostatic fat was included. The TEs for the 2D S-PRESS measurements were longer than 200 ms and therefore were much longer than typical T_2 values of macromolecules.
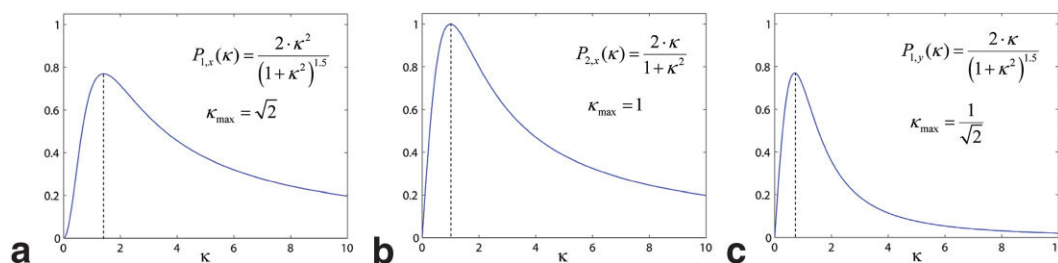

FIG. 2. Polynomial amplitude factors of the strong coupling terms in Table 1 as functions of the coupling strength $\kappa = J/\delta$: (a) $P_{1,x} = 2J^2\delta/\Lambda^3$, (b) $P_{2,x} = 2J\delta/\Lambda^2$, and (c) $P_{1,y} = 2J\delta^2/\Lambda^3$. [Color figure can be viewed in the online issue, which is available at www.interscience.wiley.com.]

In vitro measurements were carried out on a phantom solution containing 15 mM Cho, 30 mM lactate (Lac, weakly coupled), and 50 mM Cit (strongly coupled) to demonstrate the different behavior of weakly and strongly coupled spin systems. A 2D S-PRESS spectrum was acquired at TE = 438 ms using 20 TE_1 encoding steps with a spacing of $\Delta TE_1 = 20.86$ ms, yielding a nominal spectral resolution $\Delta f_1 = 2.4$ Hz in the indirect dimension. For comparison a *J*PRESS spectrum was acquired with the same nominal resolution in both f_1 and f_2.

In vivo spectra were acquired from the prostates of healthy subjects, who provided written informed consent prior to participating in the study. The voxel (14 mm $\times$ 27 mm $\times$ 14 mm = 5.3 ml) was positioned in the center of the prostate. A repetition time (TR) of 1.2 s was chosen because the T_1 relaxation time of Cit is quite short ($\approx$470 ms) and a high sensitivity for Cit detection was desired (27).

Forty equidistant TE_1 encoding steps in the range of 32.54 to (TE − 21.12) ms with 16 spectral averages each and a 16-step phase-cycling scheme were used for the 2D S-PRESS experiments, amounting to an overall scan time of 13 min. 2D S-PRESS spectra were acquired for TEs of 235 ms, 282 ms, 313 ms, and 353 ms with nominal spectral resolutions of 5.4 Hz, 4.3 Hz, 3.8 Hz, and 3.2 Hz, respectively, in the indirect dimension. These TEs were chosen on the basis of a pilot measurement that suggested intensity maxima (TE = 282 ms and TE = 353 ms) and complete cancellation (TE = 235 ms and TE = 313 ms) of the strong coupling peaks for certain TEs. For comparison a *J*PRESS spectrum was acquired using 80 encoding steps (TE range: 53.67–282 ms), eight spectral averages, and eight phase cycles. This amounts to the same overall scan time. The nominal spectral resolution in the indirect dimension (4.3 Hz) was chosen to be the same as for the S-PRESS experiment with TE = 282 ms. For the *J*PRESS acquisition, BASING water suppression was omitted to avoid a restriction to long TEs and an associated loss of sensitivity. Considerable oversampling in the indirect dimension was necessary to prevent impairment of the 2D spectra by back-folded peak tails of the residual water signal.

Three in vivo 2D S-PRESS spectra from the same subject, acquired with different TEs and in different scan sessions, were used to optimize the measurement protocol with respect to the TE. The coupling constant *J* and the chemical shift difference δ of the two coupled protons were determined from the Cit peak positions in the four spectra and averaged. Using these values, we optimized the 2D S-PRESS sequence for Cit detection by calculating the peak intensity dependence on the TE under in vivo conditions (see Appendix). Furthermore, the intersubject variability of *J* and δ was determined by 2D S-PRESS experiments (TE = 280 ms) on 11 healthy subjects (21−45 years old).

To investigate whether a zinc decrease in the prostate due to prostate cancer could be detected on the basis of changes in *J* and δ, we prepared two phantom solutions with approximate in vivo metabolite concentrations as found in literature (Table 2), with and without zinc ions. In two 2D S-PRESS experiments, the spectral parameters *J* and δ were determined for both phantoms.

Table 2
Literature Values for Metabolite Concentrations in the Healthy Prostate (21,25,34)*

Metabolite	Concentration [mM]	Reference
Cit	90	(21)
Cho	9	(34)
Cr	12	(34)
Lac	10.3	(25)
Spm	18	(34)
Na^+	145	(21)
K^+	61	(21)
Ca^{2+}	18	(21)
Mg^{2+}	14.7	(21)
Zn^{2+}	8.5	(21)
Cl^-	47.4	(21)

*A solution with these concentrations was used to investigate the influence of the Zn^{2+} concentration on the spectral parameters of citrate under in vivo conditions.
J = strength of the scalar coupling, δ = difference in Larmor frequencies.

Postprocessing of all acquired data was performed with in-house-written MATLAB code (The MathWorks, Inc.) and included zero-filling to 512 samples in t_1 and 2048 samples in t_2, a 2D Fourier transformation of the acquired data, and 1.5 Hz Gaussian filtering in both f_1 and f_2. All spectra in this paper are presented in magnitude mode as logarithmically scaled color plots.

RESULTS

The results of the in vitro experiments are presented in Fig. 3. The *J*PRESS spectrum (a) shows a simple splitting of the Lac resonance (two peaks separated by $J \approx 7$ Hz in f_1) and the typical multiplet of eight peaks for Cit. Substituting TE_2 by TE − TE_1 in the analytical terms of Table 1, expanding the trigonometric expressions and collecting contributions with a TE dependence yields resonances at $f_1 = \{\pm J/2, \pm \Lambda/2 \pm J/2, \pm \Lambda/2 \mp J/2\}$ and thus confirms the results from numerical simulations (17). In the 2D S-PRESS spectrum (b), the Lac resonance does not show a line-splitting along f_1. The Cit signal consists of the typical quartet at $f_1 = 0$ Hz, which is also observed in 1D PRESS, and two doublets at $f_1 = \pm \Lambda/2$ (henceforth called "strong coupling peaks"). The resonance frequencies of these peaks in f_2 correspond to those observed in 1D PRESS spectra. The spectral parameters of Cit were determined from the positions of the strong coupling peaks in f_1 and f_2: $J = 15.13$ Hz, δ = 14.34 Hz, $\Lambda = 20.84$ Hz.

Figure 4 shows an in vivo *J*PRESS spectrum (a) with TE ranging from 53.67 to 282 ms and a 2D S-PRESS spectrum (b) with TE = 282 ms. Both spectra have a nominal spectral resolution of 4.3 Hz in the f_1 dimension. In both spectra, Cho, Cr, and Cit resonances are visible. Additionally, the *J*PRESS spectrum shows a Spm multiplet around 3.1 ppm and lipid (Lip) resonances around 1.3 ppm. Because of their short T_2 relaxation time, those metabolites are not visible in the 2D-SPRESS spectrum, which does not contain short-TE data. The multiplet pattern of Cit is similar to the in vitro case (Fig. 3). Only the relative signal intensities of the *J*PRESS peaks are different. The following in vivo Cit parameters were determined as averaged
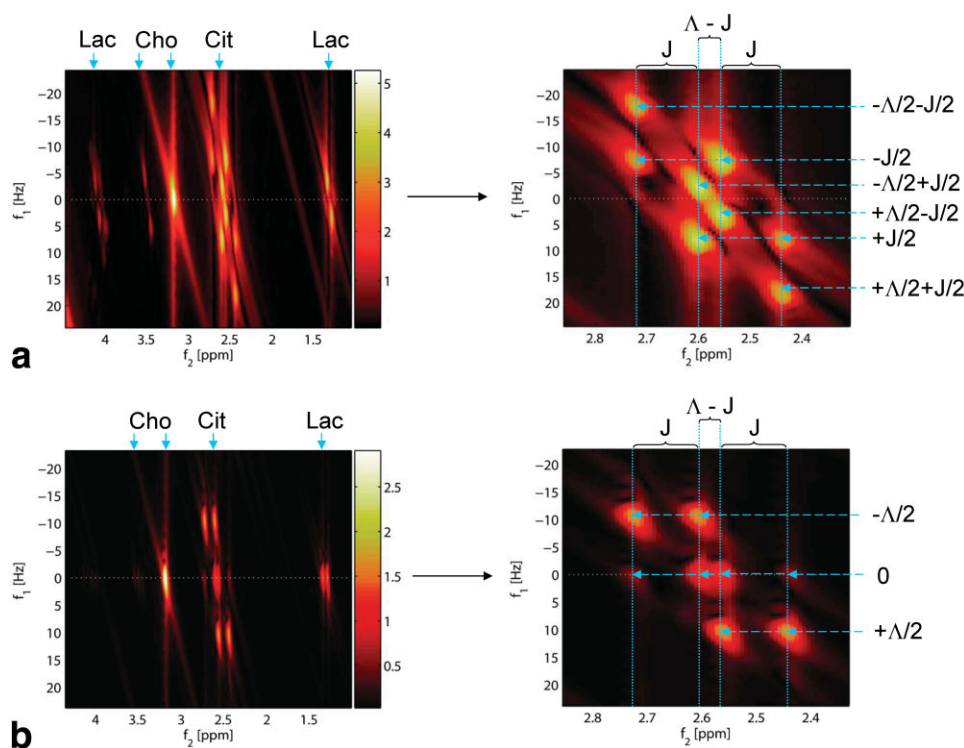
FIG. 3. *J*PRESS (**a**) and 2D S-PRESS (**b**) magnitude spectra (acquired at 3T from a phantom solution containing 15 mM Cho, 30 mM Lac, and 50 mM Cit). The *J*PRESS experiment contained 80 TE encoding steps in the range of 41.58–438 ms. The 2D-SPRESS experiment (TE = 438 ms) contained 20 TE_1 encoding steps in the range of 25.96–422.40 ms. The Cit multiplets with peak assignments are shown in zoomed sections (right graphs). [Color figure can be viewed in the online issue, which is available at www.interscience.wiley.com.]

values from this and two other 2D S-PRESS spectra acquired from the same subject: $J = (15.77 \pm 0.20)$ Hz, $\delta = (19.94 \pm 0.40)$ Hz, $\Lambda = (25.42 \pm 0.66)$ Hz. Figure 5 shows two cross sections through the 2D S-PRESS spectrum at the frequencies $f_1 = 0$ Hz and $f_1 = -12.7$ Hz. The cross section at $f_1 = 0$ Hz shows four resonance lines and looks similar to a usual PRESS spectrum acquired with the same TE. In the cross section at $f_1 = -\Lambda/2 = -12.7$ Hz, only a Cit doublet is visible at the two leftmost Cit resonance frequencies in f_2. These two peaks are separated by $\Delta f_2 = J$.

The intensity modulation of the strong coupling peaks was determined according to Eq. [4] with the measured in vivo parameters J and δ. The intensity graph (Fig. 6) shows zero-crossings for TE = $\{n \cdot 2\pi/\Lambda, n \in N\}$. We verified the accuracy of the determined spectral parameters by acquiring additional 2D S-PRESS spectra with TEs of 235 ms, 313 ms, and 353 ms (Fig. 7). For TE = 235 ms and TE = 313 ms, the strong coupling peaks of Cit are expected to have zero intensity, and indeed they vanished at these specific TEs. The maxima of the intensity graph in Fig. 6 are preferable TEs for 2D S-PRESS in the human prostate. The TE should be large enough to yield the required spectral resolution in f_1 and short enough to avoid too much signal loss due to T_2 relaxation. Therefore, TE = 278 ms and TE = 353 ms are most appropriate for S-PRESS prostate spectroscopy.

The spectral parameters of Cit (J and δ) for 11 healthy subjects are listed in Table 3. They yield mean values of $J = (15.99 \pm 0.49)$ Hz and $\delta = (19.99 \pm 0.70)$ Hz. The intersubject standard deviation (SD) is slightly larger than the SD due to different voxel positions and measurement imperfections only.

The 2D S-PRESS experiments with the two prostate phantom solutions yielded the following spectral parameters:

1. Phantom solution with zinc ions (8.5 mM, corresponding to healthy tissue): $J = 15.97$ Hz, $\delta = 18.62$ Hz.
2. Phantom solution without zinc ions (corresponding to cancerous tissue): $J = 15.84$ Hz, $\delta = 18.63$ Hz.

DISCUSSION

2D S-PRESS facilitates the unequivocal detection and quantification of strongly coupled metabolites. The combination of 2D spectroscopy techniques with PRESS localization is an obvious and promising approach since no additional pulses or gradients are required and the technique is fairly robust. Spreading the spectral information into a second dimension helps to disentangle overcrowded spectra and improve the resolution of coupled resonances. *J*PRESS has been established as a useful method for detecting *J*-coupled metabolites because it helps to distinguish coupled from uncoupled resonances. Furthermore, it provides better spectral resolution in the indirect dimension, where the line-widths are governed only by T_2 decay and not by field inhomogeneities. The application of a maximum-echo sampling scheme (24) tilts the peak tail of the residual water resonance away from the f_2 axis and prevents them from contaminating the spectral region of interest (ROI).

However, *J*PRESS spectra can be relatively complex, especially when strongly coupled spins are involved, giving rise to additional peaks in the spectrum. This also hampers the determination of exact peak positions in f_1 (Fig. 4a). For this reason Thrippleton et al. (19) devised several strategies to suppress these strong coupling peaks in *J*PRESS and correlation spectroscopy (COSY) experiments. The 2D S-PRESS method represents a complementary approach that enables strongly coupled metabolites to be identified on the basis of their strong coupling peaks. In
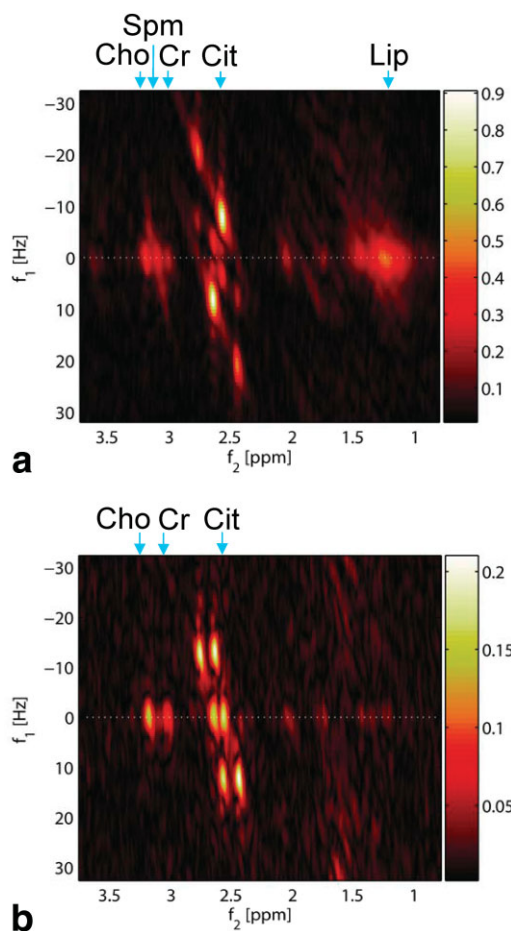
FIG. 4. In vivo *J*PRESS (**a**) and 2D S-PRESS (**b**) magnitude spectra acquired at 3T from the prostate of a healthy subject. The *J*PRESS experiment contained 80 TE encoding steps in the range of 53.67–282 ms. The 2D-SPRESS experiment (TE = 282 ms) contained 40 TE$_1$ encoding steps in the range of 32.54–260.36 ms. Detected metabolites: Cho, Cit, Cr, Lip, and Spm. [Color figure can be viewed in the online issue, which is available at www.interscience.wiley.com.]

the case of an AB spin system, the 2D S-PRESS sequence gives rise to four strong coupling peaks of equal intensity at one characteristic frequency: $f_1 = \pm \Lambda/2$. Thus, strongly coupled metabolites can easily be distinguished from uncoupled and weakly coupled ones, which resonate only at $f_1 = 0$ Hz. A cross section through the 2D S-PRESS spectrum at $f_1 = \pm \Lambda/2$ can be used for visual inspection and
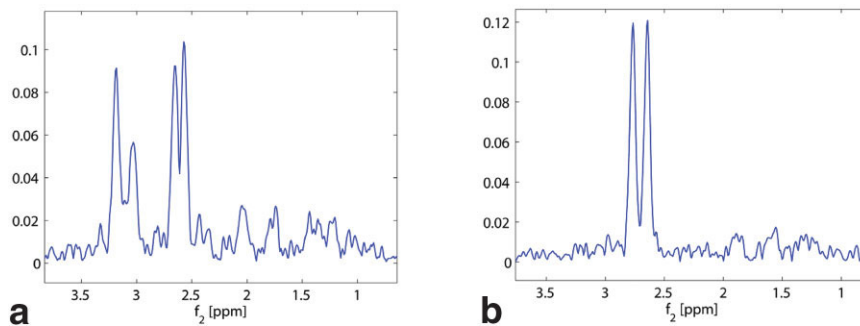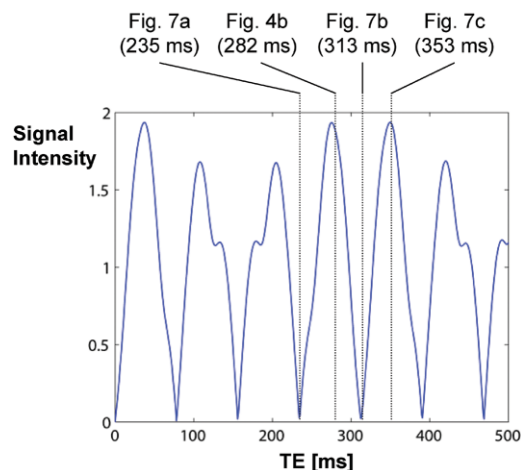

FIG. 6. In vivo signal intensity of the strong coupling S-PRESS peaks at $f_1 = \pm \Lambda/2\pi$ as a function of TE, neglecting T_2 relaxation. The TEs, for which 2D S-PRESS spectra were acquired, are indicated with dotted lines: TE = 235 ms, 282 ms, 313 ms, and 353 ms (see Figs. 4b and 7a–c). [Color figure can be viewed in the online issue, which is available at www.interscience.wiley.com.]

quantification of the Cit resonance (Fig. 5b). This particular choice of a cross section is equivalent to the S-PRESS difference editing approach presented by Gambarota et al. (20). A cross section at $f_1 = 0$ Hz, as presented in Fig. 5a, corresponds to the integral over the 2D time domain data along t_1 with a subsequent 1D Fourier transformation. This is analogous to a TE-averaged spectrum, which can be retrieved from a *J*PRESS spectrum as a cross section at $f_1 = 0$ Hz. Cross sections at $f_1 = \pm \Lambda/2$ can be reconstructed by multiplying the 2D time domain data with the linear phase factor $\exp(i \cdot \varphi)$ (with $\varphi = \pm \pi \Lambda t_1$) prior to integration along t_1 and Fourier transformation. For S-PRESS difference editing, two spectra are acquired with TE$_1 = \tau_1$ and TE$_1 = \tau_2$, which are chosen such that the Cit resonances for these two particular choices of TE$_1$ have a phase difference $\Delta\varphi = 2\pi \cdot \Lambda/2 \cdot (\tau_1 - \tau_2) = \pi$ with respect to each other ($\Lambda/2$ being the modulation frequency) (20). Applying the above-mentioned linear phase factor to the 2D S-PRESS data amounts to a phase difference $\Delta\varphi = \varphi_1 - \varphi_2 = \pi\Lambda(\tau_1 - \tau_2) = \pi$ for the two acquired spectra, which corresponds to a difference editing scheme when integrating over the indirect dimension (two-point Fourier transformation). Therefore, the S-PRESS spectrum shown by Gambarota et al. (20) corresponds to a superposition of the two cross sections in the 2D S-PRESS spectrum at $f_1 = \pm \Lambda/2$.
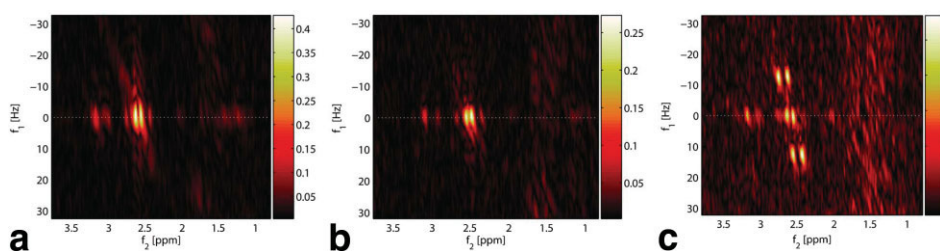

FIG. 5. Cross section through the 2D S-PRESS magnitude spectrum in Fig. 4b at $f_1 = 0$ Hz (**a**) and $f_1 = -12.7$ Hz (**b**). [Color figure can be viewed in the online issue, which is available at www.interscience.wiley.com.]

FIG. 7. 2D S-PRESS magnitude spectra acquired at 3T from the prostate of a healthy subject for TE = (**a**) 235 ms, (**b**) 313 ms, and (**c**) 353 ms. The strong coupling peaks of Cit vanish for TE = 235 ms and TE = 313 ms. [Color figure can be viewed in the online issue, which is available at www.interscience.wiley.com.]

As an additional benefit, the spectral resolution in the indirect dimension of a 2D S-PRESS spectrum is limited only by the TE_1 encoding range, and not by field inhomogeneities or T_2 relaxation as in *J*PRESS. However, the truncation in the t_1 domain requires apodization (~1–2 Hz) to prevent wiggles in the spectrum. For studies in which sensitivity is not a major concern, a sufficiently long TE can be used to obtain the desired spectral resolution in f_1. To obtain an optimal SNR for the strong coupling peaks, the TE has to be adjusted individually for every strongly coupled spin system. We found that TE = 278 ms and TE = 353 ms are preferable TEs for in vivo Cit detection. This result is in good agreement with Ref. 20, in which an optimal TE of 280 ms was suggested in the context of the original S-PRESS implementation as a difference editing approach.

As shown in this work, the spectral parameters *J* and δ of strongly coupled metabolites can be determined with reasonable precision from a 2D S-PRESS spectrum. Prostate spectroscopy using a 1D PRESS sequence does not properly resolve the Cit multiplet. Even at 3T, the two inner lines usually overlap so heavily that they appear as one peak. 2D S-PRESS enables complete and unequivocal resolution of the Cit resonances and thereby facilitates the determination of *J* and δ. The advantage of 2D S-PRESS over COSY, which is often used to determine in vivo coupling constants, is that spatial localization can be achieved at no extra cost. The determined spectral parameters (*J* = 15.99 Hz, δ = 0.157 ppm) slightly deviate from the results obtained by van der Graaf et al. (21) (*J* =

16.1 Hz, δ = 0.149 ppm), who measured a phantom solution with approximate in vivo metabolite concentrations.

It is particularly important to know the coupling parameters when they are susceptible to changes in the chemical environment of the molecule. A comparison of the measured in vitro and in vivo parameters of Cit revealed the following findings: In the Cit phantom, *J* and δ were decreased by 5% and 28% compared to their respective in vivo values in healthy prostate tissue. Even in the prostate phantom that contained all major in vivo metabolites and ions, δ was significantly reduced compared to its value in healthy subjects. However, when the 2D S-PRESS spectra from the two prostate phantoms (with and without zinc ions) were compared, there was no significant difference in δ and only a marginal difference (0.13 Hz = 0.8%) in *J*, which would not be detectable under in vivo conditions. The experiments carried out by van der Graaf et al. (21) on a phantom solution containing 90 mM Cit and 8.5 mM zinc chloride yielded much larger differences (2.4% in *J* and 5.5% in δ), which may be detectable even under in vivo conditions considering the estimates for the intra-individual error margins found in this work (1.3% for *J* and 2.0% for δ). This discrepancy reflects the fact that large concentrations of magnesium (14.7 mM) and calcium (18 mM) ions reduce the influence of zinc ions. The spectral parameters appear to depend on the total number of divalent ions, which undergoes only a small relative change, even when the concentration of zinc ions drops dramatically. Therefore the coupling evolution of Cit does not change significantly under pathological conditions. This is an important point to note because a different coupling evolution in pathological and healthy tissue might impair quantitative studies in which the Cho-to-Cit ratio in different parts of the prostate is compared (e.g., in an SI experiment) and used for clinical diagnosis. *J* and δ may also be influenced by the concentration of Spm molecules, which have opposite polarity with respect to the Cit molecules (28). It correlates with the Cit concentration and is therefore also decreased in cancerous tissue. Apart from that, *J* and δ depend on the Cit concentration itself because a reduced Cit concentration enhances the influence of the divalent ions. However, the reduced Cit and Spm concentrations under pathological conditions were not taken into account for the prostate phantom. The pH dependence of the spectral parameters (29) was not considered either, because it is primarily adjusted through the concentration of Cit and divalent ions.

Knowledge of the spectral parameters and the exact quantum-mechanical evolution is of great importance for the quantification of coupled metabolites. LCModel has been established as the most objective and robust method for metabolite quantification in recent years (30). It models

Table 3
Spectral Parameters of Citrate (*J* and δ) for Six Healthy Subjects Aged Between 21 and 45 Years, Determined With 2D S-PRESS Spectroscopy

Subject	Age	*J* [Hz]	δ [Hz]
1	22	15.77	19.94
2	22	15.78	20.61
3	27	16.35	18.91
4	26	16.35	20.94
5	24	15.87	20.08
6	27	15.40	19.93
7	22	16.35	19.91
8	21	15.58	20.73
9	25	17.05	19.22
10	45	15.46	19.03
11	44	15.90	20.58
Mean	27.7 ± 8.6	15.99 ± 0.49	19.99 ± 0.70

J = strength of the scalar coupling, δ = difference in Larmor frequencies.

the measured spectrum as a linear combination of single metabolite basis spectra, which can either be acquired in phantom experiments or simulated. This makes LCModel particularly appropriate for fitting metabolites with complicated coupling networks, for which no compact analytical description of the coupling evolution under a PRESS sequence is available. It is difficult to exactly match in vivo conditions in a phantom experiment, and therefore the coupling evolution of metabolites, such as Cit, in a phantom solution can differ from the evolution in vivo. Since this results in quantification errors, simulating the basis spectra may be a better approach for coupled resonances, such as those of Cit. For a correct simulation, however, the exact spectral parameters J and δ must be known. A 2D S-PRESS spectrum delivers these parameters at no extra cost.

Instead of fitting and quantifying cross sections through the 2D S-PRESS spectrum with LCModel, a 2D fitting method, such as ProFit (31), can be directly applied to the 2D S-PRESS spectrum to include all prior knowledge.

An alternative method for detecting strongly coupled spin systems was presented by Trabesinger et al. (32), who suggested spectral editing with a single quantum coherence filter for taurine detection. This technique exploits the fact that detectable single quantum coherences are created through the coherence transfer between the strongly coupled spins, while for uncoupled and weakly coupled spin systems only even coherence orders are produced, which are not directly observable in the acquisition. However, spectral editing techniques based on coherence pathway selection usually have an inherent signal loss of 50%. On the other hand, 2D S-PRESS requires longer TEs than common coherence filtering techniques and is therefore not the method of choice for large metabolites with very short T_2 relaxation times.

Since prostate cancer usually occurs in the peripheral zone of the prostate, single-voxel measurements, as performed in this work, are not appropriate for clinical diagnosis. However, one could increase the SNR considerably by using an endorectal coil for signal reception instead of surface coils. This might enable a combination of 2D S-PRESS with SI in order to obtain spatial distributions of metabolites over the whole prostate. Fat suppression, which is not an issue for the single-voxel approach, could be achieved with either broadband outer volume suppression (OVS) pulses or a dual-band BASING pulse, which inverts water and fat at the same time.

Analytical considerations presented in the Theory section show that Cit is an ideal metabolite for S-PRESS. Its coupling strength ensures a near-optimal signal yield at 3T, and the comparably simple signal structure of an AB spin system is appropriate for analytical investigations, which can be used to optimize the sequence. However, 2D S-PRESS may also turn out to be useful for spectroscopy in the brain, where several metabolites of interest (e.g., glutathione, GABA, myoinositol) are strongly coupled. In particular, the cysteinyl group of glutathione, which has a relatively simple coupling network (ABX), may be an interesting target metabolite. Gambarota et al. (33) recently investigated the signal modulation of glutathione with TE_1 and TE applying numerical and experimental methods. However, a compact analytical description for the signal response of an ABX spin system to a PRESS sequence would be helpful for optimizing 2D S-PRESS for glutathione detection.

CONCLUSIONS

We have shown that 2D S-PRESS is a viable alternative to the widely used *J*PRESS method for prostate spectroscopy. The technique may help to further establish MRS as a method for detecting metabolic changes associated with prostate cancer, and has the potential to be useful for spectroscopy in other anatomical regions as well.

ACKNOWLEDGMENTS

APPENDIX

The overall signal intensity of the strong coupling peaks can be calculated as the integral over the 2D magnitude spectrum. An integration over a complex spectrum f(ω) = $f_r(\omega)$ + i · $f_i(\omega)$ corresponds to the time domain signal F(t) = $F_r(t)$ + i · $F_i(t)$ at the reference point (zero point) of the FFT.

$$F(t) = \int f(\omega) \cdot \exp(i\omega t) \cdot d\omega \Rightarrow F(0) = \int f(\omega) \cdot d\omega \quad [4]$$

However, this relation is no longer valid for the magnitude data unless all resonances are in phase with respect to each other. In that case, all signals can be transferred to the real part $F_r(t)$ by rephasing the spectrum, which amounts to

$$|F(0)| = |F_r(0)| = \int |f_r(\omega)| \cdot d\omega = \int |f(\omega)| \cdot d\omega. \quad [5]$$

Only the strong coupling terms (depending on $TE_1 - TE_2$) in the in-phase magnetization expectation values (Table 1) are taken into account for the integration ($\varphi = \frac{\pi}{2}\Lambda \cdot (2 \cdot TE_1 - TE)$):

$$\langle A_y^{SC} \rangle = \langle B_y^{SC} \rangle = -2J\delta^2/\Lambda^3 \cdot \sin(\pi J \cdot TE)\sin\left(\frac{\pi}{2}\Lambda \cdot TE\right) \cdot \cos(\varphi)$$

$$= F_{1,y}(TE) \cdot \cos(\varphi) \quad [6a]$$

$$\langle A_x^{SC} \rangle = -\langle B_x^{SC} \rangle =$$

$$-2J^2\delta/\Lambda^3 \cdot \cos(\pi J \cdot TE)\sin\left(\frac{\pi}{2}\Lambda \cdot TE\right) \cdot \cos(\varphi)$$

$$-2J\delta/\Lambda^2 \cdot \sin(\pi J \cdot TE)\sin\left(\frac{\pi}{2}\Lambda \cdot TE\right) \cdot \sin(\varphi)$$

$$= F_{1,x}(TE) \cdot \cos(\varphi) + F_{1,x}(TE) \cdot \sin(\varphi) \quad [6b]$$

Because of $\langle A_x^{SC} \rangle = -\langle B_x^{SC} \rangle$, the signal intensities have to be calculated separately for two spins. Due to the factor

$\sin(\varphi)$ in the *x*-magnetization amplitude, the strong coupling peaks in the positive ($f_1 > 0$) and negative ($f_1 < 0$) half-plane are out of phase with respect to each other and must be integrated separately. This requires splitting up the trigonometric factors $\cos(\varphi)$ and $\sin(\varphi)$ into exponential expressions:

$$\cos(\varphi) = \frac{1}{2}(\exp(i\varphi) + \exp(-i\varphi)) \quad [7a]$$

$$\sin(\varphi) = \frac{1}{2i}(\exp(i\varphi) - \exp(-i\varphi)) \quad [7b]$$

All terms with $\exp(i\varphi)$ give rise to resonances in the positive half-plane, while all terms with $\exp(-i\varphi)$ give rise to resonances in the negative half-plane. Assuming quadrature detection, the overall signal turns out to be the sum of four contributions:

$$I_{sc} = |\langle A_-^{sc}\rangle|_{f_1>0} + |\langle A_-^{sc}\rangle|_{f_1<0} + |\langle B_-^{sc}\rangle|_{f_1>0} + |\langle B_-^{sc}\rangle|_{f_1<0}$$

$$= \left|\frac{1}{2}(F_{1,x} - i(F_{2,x} + F_{1,y}))\cdot\exp(i\varphi)\right|$$

$$+ \left|\frac{1}{2}(F_{1,x} + i(F_{2,x} - F_{1,y}))\cdot\exp(-i\varphi)\right|$$

$$= \left|\frac{1}{2}(-F_{1,x} + i(F_{2,x} - F_{1,y}))\cdot\exp(i\varphi)\right|$$

$$+ \left|\frac{1}{2}(-F_{1,x} - i(F_{2,x} + F_{1,y}))\cdot\exp(-i\varphi)\right|$$

$$= \sqrt{F_{1,x}^2 + (F_{2,x} + F_{1,y})^2} + \sqrt{F_{1,x}^2 + (F_{2,x} - F_{1,y})^2}. \quad [8]$$

REFERENCES

1. Kurhanewicz J, Swanson MG, Nelson SJ, Vigneron DB. Combined magnetic resonance imaging and spectroscopic imaging approach to molecular imaging of prostate cancer. J Magn Reson Imaging 2002;16:451–463.
2. Scheidler J, Hricak H, Vigneron DB, Yu KK, Sokolov DL, Huang LR, Zaloudek CJ, Nelson SJ, Carroll PR, Kurhanewicz J. Prostate cancer: Localization with three-dimensional proton MR spectroscopic imaging—clinicopathologic study. Radiology 1999;213:473–480.
3. Costello LC, Franklin RB, Narayan P. Citrate in the diagnosis of prostate cancer. Prostate 1999;38:237–245.
4. Garcia-Segura JM, Sanchez-Chapado M, Ibarburen C, Viano J, Angulo JC, Gonzalez J, Rodriguez-Vallejo JM. In vivo proton magnetic resonance spectroscopy of diseased prostate: spectroscopic features of malignant versus benign pathology. Magn Reson Imaging 1999;17:755–765.
5. Kurhanewicz J, Vigneron DB, Hricak H, Narayan P, Carroll P, Nelson SJ. Three-dimensional H-1 MR spectroscopic imaging of the in situ human prostate with high (0.24-0.1-cm(3)) spatial resolution. Radiology 1996; 198:795–805.
6. Bottomley PA. Spatial localization in NMR-spectroscopy in vivo. Ann NY Acad Sci 1987;508:333–348.
7. Frahm J, Merboldt KD, Hanicke W. Localized proton spectroscopy using stimulated echoes. J Magn Reson 1987;72:502–508.
8. Mulkern RV, Bowers JL, Peled S, Kraft RA, Williamson DS. Citrate signal enhancement with a homonuclear J-refocusing modification to double-echo PRESS sequences. Magn Reson Med 1996;36:775–780.
9. Schick F, Bongers H, Kurz S, Jung WI, Pfeffer M, Lutz O. Localized proton MR spectroscopy of citrate in vitro and of the human prostate in vivo at 1.5-T. Magn Reson Med 1993;29:38–43.
10. Schick F, Straubinger K, Machann J, Nagele T, Bunse M, Klose U, Lutz O. Sequence parameters of double spin-echo sequences affect quantification of citrate. Magn Reson Imaging 1996;14:663–672.
11. Straubinger K, Schick F, Lutz O. Pulse angle dependence of double-spin-echo proton NMR spectra of citrate—theory and experiments. J Magn Reson Ser B 1996;110:188–194.
12. Trabesinger AH, Meier D, Dydak U, Lamerichs R, Boesiger P. Optimizing PRESS localized citrate detection at 3 Tesla. Magn Reson Med 2005;54:51–58.
13. Wilman AH, Allen PS. The response of the strongly coupled AB system of citrate to typical H-1 MRS localization sequences. J Magn Reson Ser B 1995;107:25–33.
14. van der Graaf M, Jager GJ, Heerschap A. Removal of the outer lines of the citrate multiplet in proton magnetic resonance spectra of the prostatic gland by accurate timing of a point-resolved spectroscopy pulse sequence. Magn Reson Mater Phy Biol Med 1997;5:65–69.
15. Ryner LN, Sorenson JA, Thomas MA. Localized 2D J-resolved H-1 MR spectroscopy—strong-coupling effects in-vitro and in-vivo. Magn Reson Imaging 1995;13:853–869.
16. Swanson MG, Vigneron DB, Tran TKC, Sailasuta N, Hurd RE, Kurhanewicz J. Single-voxel oversampled J-resolved spectroscopy of in vivo human prostate tissue. Magn Reson Med 2001;45:973–980.
17. Yue K, Marumoto A, Binesh N, Thomas MA. 2D JPRESS of human prostates using an endorectal receiver coil. Magn Reson Med 2002;47: 1059–1064.
18. Kim DH, Margolis D, Xing L, Daniel B, Spielman D. In vivo prostate magnetic resonance spectroscopic imaging using two-dimensional J-resolved PRESS at 3 T. Magn Reson Med 2005;53:1177–1182.
19. Thripleton MJ, Edden RAE, Keeler J. Suppression of strong coupling artefacts in J-spectra. J Magn Reson 2005;174:97–109.
20. Gambarota G, van der Graaf M, Klomp D, Mulkern RV, Heerschap A. Echo-time independent signal modulations using PRESS sequences: a new approach to spectral editing of strongly coupled AB spin systems. J Magn Reson 2005;177:299–306.
21. van der Graaf M, Heerschap A. Effect of cation binding on the proton chemical shifts and the spin-spin coupling constant of citrate. J Magn Reson Ser B 1996;112:58–62.
22. Kay LE, McClung RED. A product operator description of AB and ABX spin systems. J Magn Reson 1988;77:258–273.
23. Macura S, Brown LR. Improved sensitivity and resolution in two-dimensional homonuclear J-resolved NMR-spectroscopy of macromolecules. J Magn Reson 1983;53:529–535.
24. Schulte RF, Lange T, Beck J, Meier D, Boesiger P. Improved two-dimensional J-resolved spectroscopy. NMR Biomed 2006;19:264–270.
25. Males RG, Vigneron DB, Star-Lack O, Falbo SC, Nelson SJ, Hricak H, Kurhanewicz J. Clinical application of BASING and spectral/spatial water and lipid suppression pulses for prostate cancer staging and localization by in vivo 3D H–1 magnetic resonance spectroscopic imaging. Magn Reson Med 2000;43:17–22.
26. Star-Lack J, Nelson SJ, Kurhanewicz J, Huang LR, Vigneron DB. Improved water and lipid suppression for 3D PRESS CSI using RF band selective inversion with gradient dephasing (BASING). Magn Reson Med 1997;38:311–321.
27. Scheenen TWJ, Gambarota G, Weiland E, Klomp DWJ, Futterer JJ, Barentsz JO, Heerschap A. Optimal timing for in vivo H-1-MR spectroscopic imaging of the human prostate at 3T. Magn Reson Med 2005; 53:1268–1274.
28. Lynch MJ, Nicholson JK. Proton MRS of human prostatic fluid: correlations between citrate, spermine, and myo-inositol levels and changes with disease. Prostate 1997;30:248–255.
29. Moore GJ, Sillerud LO. The pH-dependence of chemical-shift and spin-spin coupling for citrate. J Magn Reson Ser B 1994;103:87–88.
30. Provencher SW. Estimation of metabolite concentrations from localized in-vivo proton NMR-spectra. Magn Reson Med 1993;30:672–679.
31. Schulte RF, Boesiger P. ProFit: two-dimensional prior-knowledge fitting of J-resolved spectra. NMR Biomed 2006;19:255–263.
32. Trabesinger AH, Mueller DC, Boesiger P. Single-quantum coherence filter for strongly coupled spin systems for localized H-1 NMR spectroscopy. J Magn Reson 2000;145:237–245.
33. Gambarota G, Mlynarik V, Gruetter R, Liptaj T. A novel approach to spectral editing of glutathione at 7 Tesla using echo-time independent signal modulations in PRESS sequence. In: Proceedings of the 14th Annual Meeting of ISMRM, Seattle, WA, USA. p 3058.
34. van der Graaf M, Schipper RG, Oosterhof GO, Schalken JA, Verhofstad AA, Heerschap A. Proton MR spectroscopy of prostatic tissue focused on the detection of spermine, a possible biomarker of malignant behavior in prostate cancer. MAGMA 2000;10:153–159.